Atomic Scale Growth Dynamics of Nanocrystals within Carbon Nanotubes

Jamie H. Warner,* Simon R. Plant, Neil P. Young, Kyriakos Porfyrakis, Angus I. Kirkland, and G. Andrew D. Briggs

Department of Materials, University of Oxford, Parks Road, Oxford OX1 3PH, United Kingdom

ABSTRACT The confined interior region of carbon nanotubes has proved to be an effective "nano-test-tube" to conduct chemical reactions in a restricted volume. It also benefits from being thin and relatively transparent to electrons, enabling structural characterization using high-resolution transmission electron microscopy. This permits real-time monitoring of chemical reactions with atomic resolution. Here, we have studied the dynamics of single Pr atoms released from $Pr_2@C_{72}$ metallofullerenes. We show that the Pr atoms form small nanoclusters that subsequently coalesce to ordered, stable nanocrystals within the confines of a carbon nanotube. This process has been tracked *in situ* with atomic-resolution using low-voltage aberration-corrected high-resolution transmission electron microscopy. We reveal that nanocrystal formation within a nanotube does not generally occur by the addition of single atoms to one pre-existing cluster but rather through aggregation of several smaller clusters. These results provide some of the deepest insights into the dynamics of single-atom behavior in the solid state.

KEYWORDS: peapods · nanotubes · nanocrystals · HRTEM · aberration-corrected

The hollow region inside a carbon nanotube has been demonstrated to be an effective reaction vessel for filling with molecular nanomaterials and examination of changes to their structure,[1] often after the application of energy to the system in the form of heat.[2−6] In several cases, these structural transformations have been captured in real time.[2,7−11] Recent advances in low-voltage aberration-corrected high-resolution transmission electron microscopy (LV-AC-HRTEM) enables atomic resolution imaging of carbon-based nanomaterials without inducing significant damage.[12,13] Electron beam damage of materials using electron microscopy is often perceived as a problem, but under the right conditions, it can be beneficial for studying *in situ* structural transformations.[14−17] The three main forms of electron beam damage are knock-on damage, radiolysis, and heating.[18] LV-AC-HRTEM with an accelerating voltage of 80 kV is below the knock-on damage threshold for saturated sp^2-bonded carbon atoms in nanotubes, and the excellent thermal conductivity of carbon nanotubes makes heating effects negligible.[19] Radiolysis is an inelastic scattering process mainly involving electron−electron interactions that results in the breaking of chemical bonds. However, radiolysis of clean large diameter multiwalled carbon nanotubes is not a problem due to the large reservoir of electrons associated with metallic nanotubes. This leads to the scenario where 80 kV electron beam irradiation can be used to preferentially induce structural transformations of materials encapsulated within carbon nanotubes without the electron beam directly modifying the nanotube host.[11,20]

When peapods (fullerenes inside nanotubes) are irradiated with an 80 kV electron beam, the fullerenes coalesce and eventually form a high-quality, smaller diameter nanotube within the original host nanotube.[11] If metallofullerenes are used, the metal atoms are confined to the inner region of the newly formed nanotube.[11] The presence of metal atoms within the carbon structure can also influence these structural transformations.[8,10] Studies into the rupturing of endohedral fullerene cages and the subsequent release of metal atoms have been previously performed.[10,11,21−23] Urita *et al.* provided the first clear evidence of the single-atom migration of Tb, Gd, and Ce from fullerene to fullerene, but the use of a 120 kV accelerating voltage meant that knock-on damage could not be precluded as a mechanism behind the observed process.[21] We have previously reported that when peapods containing $La@C_{82}$ were irradiated with an electron beam at 80 kV accelerating voltage they coalesce and form an internal nanotube with the metal atoms confined in the inner region.[11] In most cases, the La atoms remained within the nanotube host, and if the diameter was large enough, small crystals formed. However, the crystal formation mechanism was not elucidated. Similar experiments with

*Address correspondence to jamie.warner@materials.ox.ac.uk.

Received for review November 23, 2010 and accepted January 12, 2011.

Published online January 26, 2011
10.1021/nn1031802

$Dy@C_{82}$ peapods have also been reported (at 80 kV), but the Dy atoms ruptured the nanotube host and only disordered clusters were observed.[10] This was attributed to the presence of Dy^{4+} and its inability to form a carbide phase to stabilize the structure.[10]

Kitaura *et al.* have shown that highly ordered crystalline phases of metals can be formed inside nanotube hosts by heating peapods containing metallofullerenes to high temperatures under vacuum.[6] The resulting structure formed by this approach is controlled by the diameter of the nanotube host, and when the nanotube diameter is reduced, it leads to 1D metallic wires.[3] Filling nanotubes with metals and metal halides has been extensively studied.[24] The interatomic distances of metal atoms are usually large enough that aberration correction is not needed to obtain the lattice structure of the metal crystals. Rotational twists and motion of crystals have also been reported.[25,26] Experimental evidence for the mechanisms underlying nanocrystal formation inside nanotubes still remains relatively unexplored. This is due to the lack of experimental *in situ* studies that track the process at the single-atom level in real time, and most insight has been acquired through theoretical modeling.[27] Here, we present the most detailed study to date of the mechanisms by which single atoms form clusters that lead to the formation of stable nanocrystals inside carbon nanotubes. This process has been tracked with single-atom resolution within the stable confines of multiwalled carbon nanotubes utilizing the bimetal endohedral fullerene, $Pr_2@C_{72}$, as the metal source.[28,29] It is possible that the $Pr_2@C_{72}$ might in fact be $Pr_2C_2@C_{70}$; however, the NMR and UV−vis−NIR absorption spectrum shows stronger support for a C_{72} cage.[28] Here, we focus on possible assignments for a $Pr@C_{72}$ cage structure.

RESULTS AND DISCUSSION

Figure 1 shows $Pr_2@C_{72}$ metallofullerenes (MFs) encapsulated within a double-walled carbon nanotube (DWNT). The contrast from the two Pr atoms is clearly seen, and all the MFs are orientated with their long axis parallel to the axis of the DWNT. This orientation enables observation of both Pr atoms for nearly all the MFs. This alignment is most likely due to the narrow diameter of the DWNT and the restriction it imposes on the ability of the MFs to rotate in arbitrary directions, similar to the effect of aligned C_{70} in SWNTs.[30] The alignment of the $Pr_2@C_{72}$ in the nanotube also enables the distance between the two Pr atoms inside the cage to be measured, giving an average Pr−Pr separation of ~0.37 nm. Panels a−f of Figure 1 show changes in the peapods due to electron beam irradiation. A single Pr atom, indicated with a red arrow in Figure 1a−f, is observed to escape the C_{72} cage and enter the interior region of the inner nanotube. Some movement of the $Pr_2@C_{72}$ MFs is also observed. In Figure 1e,f, the preferred orientation of the MF indicated with a yellow arrow changes. The shape of the C_{72} cage is not spherical but oblong, and measurement of the ratio of the long/short axis of the $Pr_2@C_{72}$ from Figure 1 gives values of 1.3−1.4.

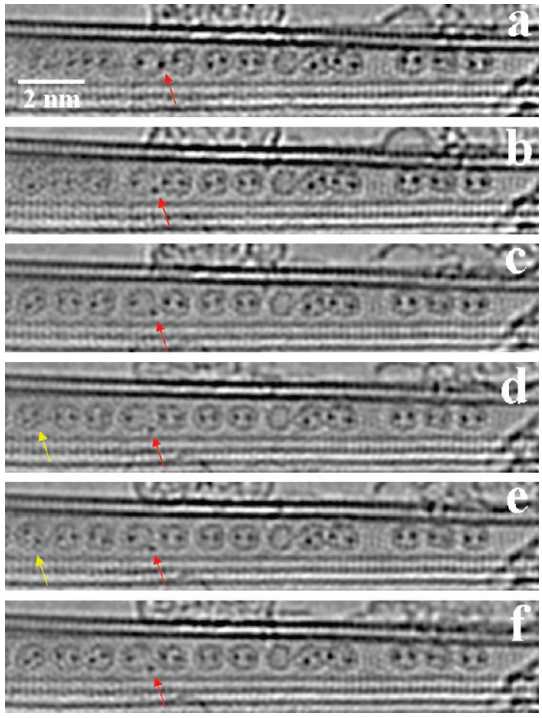

Figure 1. Time series (a−f) of HRTEM images of $Pr_2@C_{72}$ DWNT peapods under 80 kV electron beam irradiation showing the escape of a single atom indicated by the red arrow and the controlled rotation of individual MFs indicated by the yellow arrow. Ten seconds between frames.

We have also examined the orientation of the $Pr_2@C_{72}$ in wider diameter MWNTs, such as the triple-walled carbon nanotube (TWNT) with 1.4 nm inner tube diameter shown in Figure 2. The wider diameter nanotube enables the $Pr_2@C_{72}$ to freely rotate, showing arbitrary projection relative to the incident beam direction. In Figure 2a, several of the MFs only show one spot of high contrast due to the two Pr atoms overlapping in projection. In this projection, the shape of the C_{72} cage is circular. This geometry rules out the IPR D_{6d}-C_{72} cage symmetry, which is disk-like in shape. Kato *et al.* found that $La_2@C_{72}$ had non-IPR cage structure of #10611 or possibly #10958.[31] Both non-IPR C_{72} cage structures provide good matches to the cage structures observed for the $Pr_2@C_{72}$ in Figures 1 and 2. However, it is not possible to distinguish between the two cages from our HRTEM images. Figure 2d shows an atomic model of a $Pr_2@C_{72}$ #10958 cage with the short axis perpendicular to the viewing direction. The two Pr atoms (green) overlap, while the cage has circular profile, consistent with the HRTEM image in Figure 2b. Figure 2e shows the same $Pr_2@C_{72}$ #10958 cage, with the long axis perpendicular to the viewing direction. Two Pr atoms are seen, and

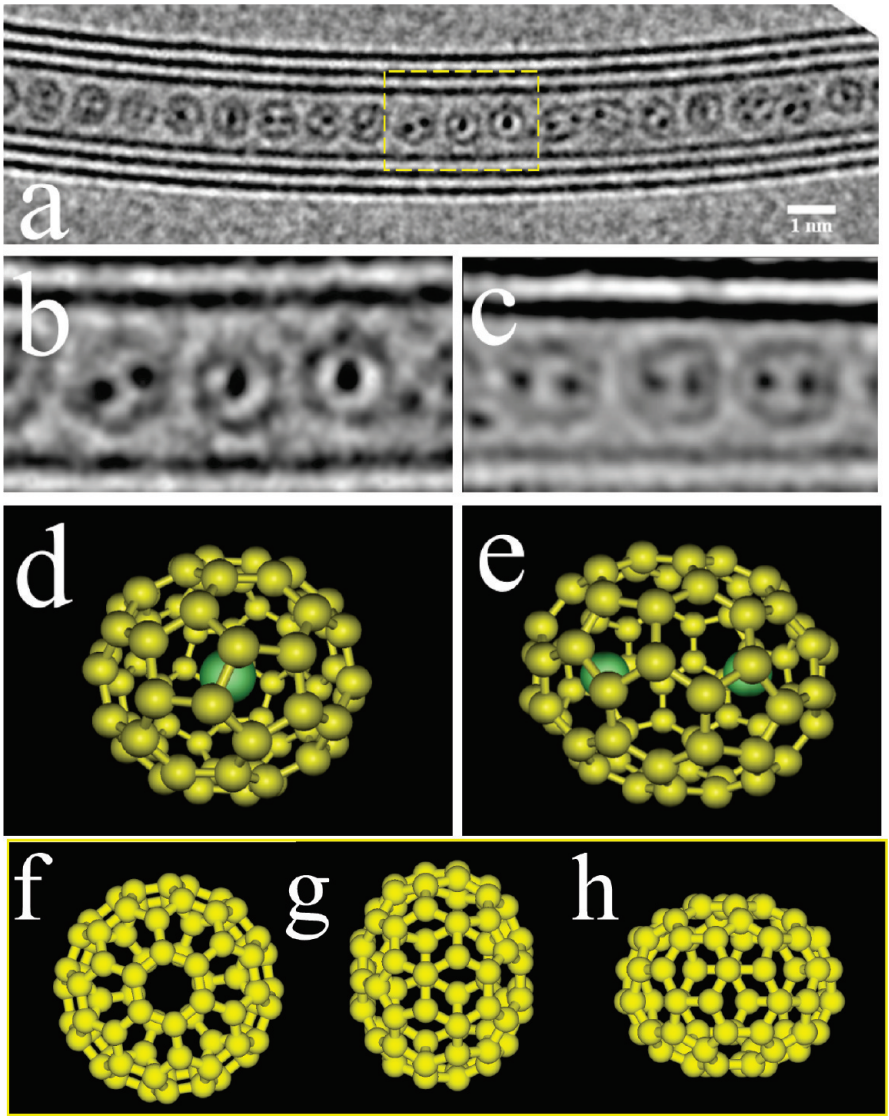

Figure 2. (a) HRTEM image of $Pr_2@C_{72}$ MFs inside a TWNT. (b) Magnified view of the region indicated with a yellow box in (a) showing the two different orientations of the $Pr_2@C_{72}$ MFs. (c) Magnified view of the aligned $Pr_2@C_{72}$ MFs from Figure 1e. (d) Atomic model of the non-IPR C_{72} #10598 with two Pr atoms (green) incorporated and the short axis perpendicular to the viewing direction. (e) Atomic model of the non-IPR C_{72} #10958 with two Pr atoms (green) incorporated and the long axis perpendicular to the viewing direction. (f) Atomic model of the IPR D_{6d}-C_{72}. (g) Model in (f) rotated 90° about the vertical axis. (h) Model in (f) rotated 90° about the horizontal axis.

the shape of the cage appears oval, consistent with the HRTEM image in Figure 2c. It is possible that other non-IPR C_{72} cages have similar profiles, but our essential point is that the cage is non-IPR, as in the case of $La_2@C_{72}$, and not the IPR D_{6d}-C_{72}. Figure 2f shows the atomic model of the IPR D_{6d}-C_{72} cage, and Figure 2g,h shows the same rotated 90° about the vertical and horizontal axes.

In Figure 1, the contrast from individual Pr atoms is not always identical. In order to further understand the HRTEM images of the peapods, multislice image simulations were performed.[32] Figure 3a shows the atomic model used for the supercell calculations for a DWNT with five $Pr_2@C_{72}$ MFs aligned with their long axis parallel to the DWNT axis. Corresponding HRTEM image simulations with 5 nm defocus as a function of decreasing microscope resolution are presented in Figure 3b–d. Figure 3e plots a line profile from the central region of Figure 3d, through the location of the Pr atoms. The minima in the gray scale intensity correspond to the dark contrast of the Pr atoms. Thus, there are five pairs of minima for the five $Pr_2@C_{72}$ metallofullerenes. Figure 3e shows that the contrast from the Pr atoms is not uniform. This is due to the position of the Pr atom relative to the atomic structure of the DWNT and explains why the contrast from a single Pr atom can appear to vary inside a carbon nanotube.

The detailed understanding of the contrast observed in the HRTEM images shown in Figures 1 and 2 enables investigation of the dynamics of individual Pr atoms within the confined region of the MWNTs.

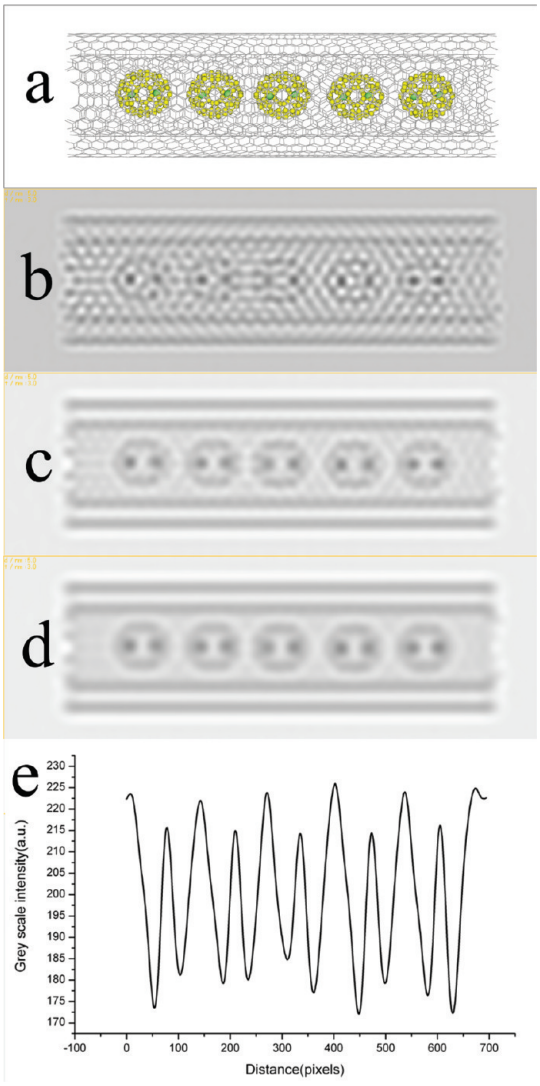

Figure 3. (a) Atomic model of the $Pr_2@C_{72}$ DWNT peapod used for the supercell HRTEM image simulation. HRTEM image simulations (5 nm defocus) with different image resolution achieved by varying the chromatic defocus spread from (b) 4 nm, (c) 10 nm, to (d) 17 nm. (e) Line profile taken horizontally across (d) in the central region containing the Pr atoms.

We have found that electron beam irradiation at 80 kV led to the fusion of the $Pr_2@C_{72}$ MFs and the formation of an inner nanotube with the metal atoms confined. This is similar to our previous report of irradiation studies of $La@C_{82}$ peapods.[11] However, in the case of $Pr_2@C_{72}$, there are twice as many heavy metal atoms. Figure 4i presents a time series of HRTEM images showing the movement of single Pr atoms within the inner nanotube after 2 min of electron-beam-induced coalescence at 80 kV. The time between images is 10 s. This demonstrates the ability to track the position of single atoms as a function of time. At this initial stage, the atoms are distributed throughout the nanotube and hop between positions of fixed stability.

Figure 4ii shows a TWNT filled with $Pr_2@C_{72}$ and irradiated with an electron beam at 80 kV. In Figure 4ii,a, the outline of each MF is barely resolved due to the movement of the MFs. The time between frames 4ii,a and 4ii,b is approximately 1 min. Figure 4ii,b shows that several of the $Pr_2@C_{72}$ have fused together and a large number of Pr atoms are located within the newly formed inner tube. The packing of MFs in Figure 4ii,a leads to approximately 19 $Pr_2@C_{72}$ within the region imaged, corresponding to 38 Pr atoms. This correlates with the number of high contrast spots observable in Figure 4ii,b. The Pr atoms are mobile and thus move back and forth within the confined region of the inner tube. Pairing of Pr atoms is also observed, and small cluster formation occurs toward the end of the time sequence of images. In Figure 4ii,c, after a further minute of irradiation, clearly defined high contrast spots are observed that are more intense and wider than those observed in Figure 4ii,b. The number of spots has also reduced. These observations are indicative of the formation of Pr clusters, confirmed by Figure 4ii,d, which shows after another minute of irradiation three well-defined clusters, indicated with arrows. Ten seconds later, Figure 4ii,e, these clusters have moved, demonstrating that it is not just single Pr atoms that are mobile but also the clusters. Figure 4ii,f shows that after a further 10 s a cluster starts to exhibit initial signs of ordering and long-range crystallinity, indicated with an arrow. This reveals that single Pr atoms are released from their C_{72} cages and are mobile, moving around the confined environment of the inner nanotube until encountering other Pr atoms, after which they nucleate small clusters that are also mobile and then subsequently crystallize as the cluster size increases.

Figure 5 shows a continuation of the time series presented in Figure 4ii, demonstrating the transformation of these small clusters into a single uniform nanocrystal. The time between frames is 10 s. In Figure 5a, four small clusters are observed, indicated with arrows. They are initially random and are mobile and undergo continuous structural transformations. After 10 s, the two inner clusters coalesce to form a larger single cluster. These three clusters then remain relatively unchanged until Figure 5e, in which the middle cluster has moved and joined the cluster toward the right. With further irradiation, Figure 5h, the larger cluster shows a high degree of order. Overall, this time series of images shows that the formation of nanocrystals within the confined region inside a nanotube occurs by first the assembly of small clusters and then the coalescence of these smaller clusters to form a larger structure, rather than the atom by atom addition of Pr to a single cluster.

We have observed that once an ordered nanocrystal formed it was robust to further electron beam irradiation and did not fragment into smaller subclusters. However, the nanocrystal was mobile within the inner nanotube and exhibited translational motion. This motion

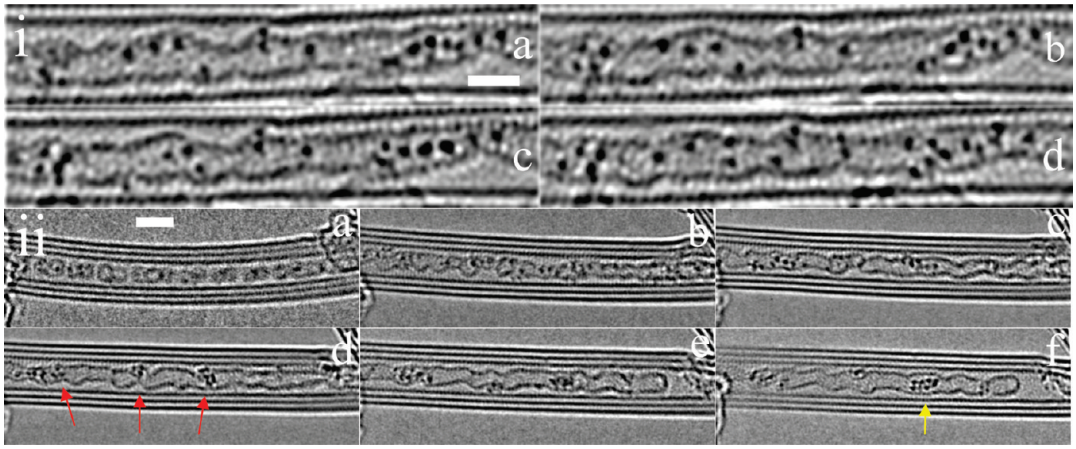

Figure 4. (i) Time series (a−d) of HRTEM images showing the movement of single Pr atoms within the inner nanotube. Time between images is 10 s. Scale bar in (a) indicates 1 nm. (ii) Sequence of HRTEM images of $Pr_2@C_{72}$ in a TWNT under electron beam irradiation for (a) 0 min, (b) 1 min, (c) 2 min, (d) 3 min, with arrows indicating clusters (e) 3 min + 10 s, (f) 3 min + 20 s. The yellow arrow indicates a region showing long-range crystallinity. Scale bar in (a) is 2 nm.

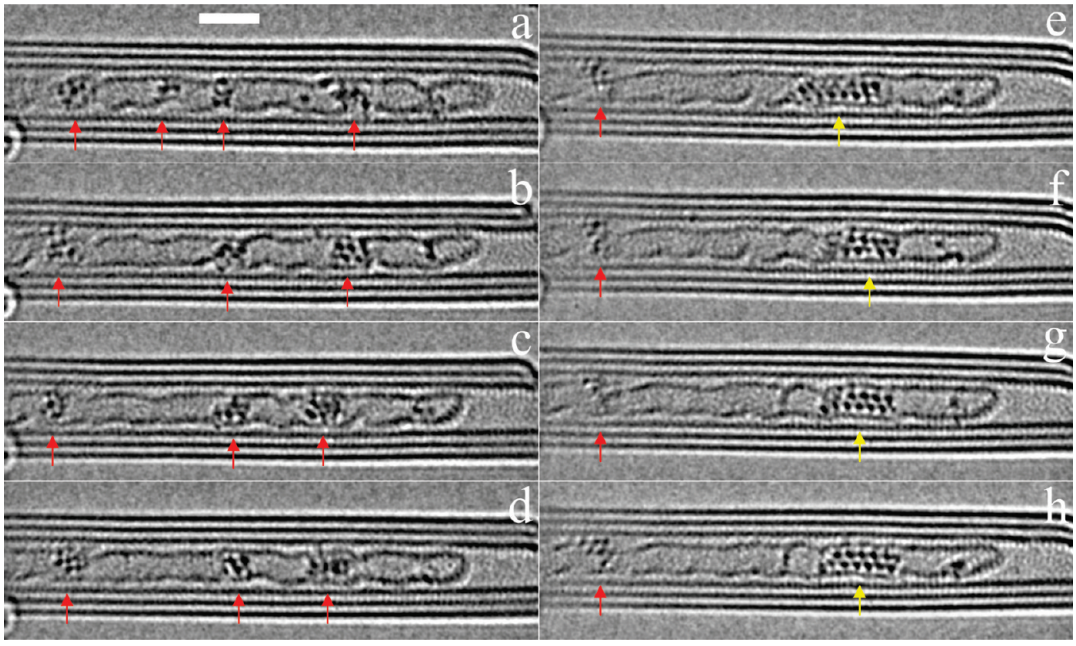

Figure 5. Time series of HRTEM images showing the coalescence of clusters to form a nanocrystal. Time between frames is 10 s. Red arrows indicate clusters, and yellow arrows indicate long-range crystallinity. Between (a) and (b), clusters reduce from 4 to 3 *via* coalescence. Rotation of cluster state is observed between (b) and (d). Merging of two clusters to form one nanocrystal is observed between (d) and (e). Nanotube host remains undamaged throughout the process. Scale bar in (a) is 2 nm.

was constrained by the narrow diameter of the inner nanotube, indicated with an arrow in Figure 6f. Although the nanocrystal did not fragment into smaller clusters, the Pr atoms were still observed to be dynamic within the nanocrystal. Figure 6 shows examples of the real-time atomic structural rearrangements that occur in the system, with 10 s between frames. In Figure 6b,f, g,i,j,k, the same projection of the Pr nanocrystal is observed. This projection shows strong contrast at the atomic columns and indicates it is stable for the 2 s duration required to capture the image. Between these periods of fixed stability, the ability to resolve the position of individual Pr atoms has diminished. We believe that this is due to the nanocrystal rotating about an axis, parallel to the MWNT axis, leading to blurring of the atomic structure in projection. The nanocrystal rotates for a specific period and then halts with an orientation preference, as shown in Figure 6b,f, g,i,j,k. During these observations, rotation of the entire nanotube can be readily eliminated by tracking distinct features in the structure that remained fixed.

Projection of the crystal structure shown in Figure 6j matches the tetragonal $I_{4/mmm}$, PrC_2 lattice with a = 0.385 nm, c = 0.6425 nm, and a C−C distance of 0.129 nm.[33] Figure 7 shows atomic models of PrC_2 nanocrystals based on this unit cell in a MWNT. Figure 7a−d

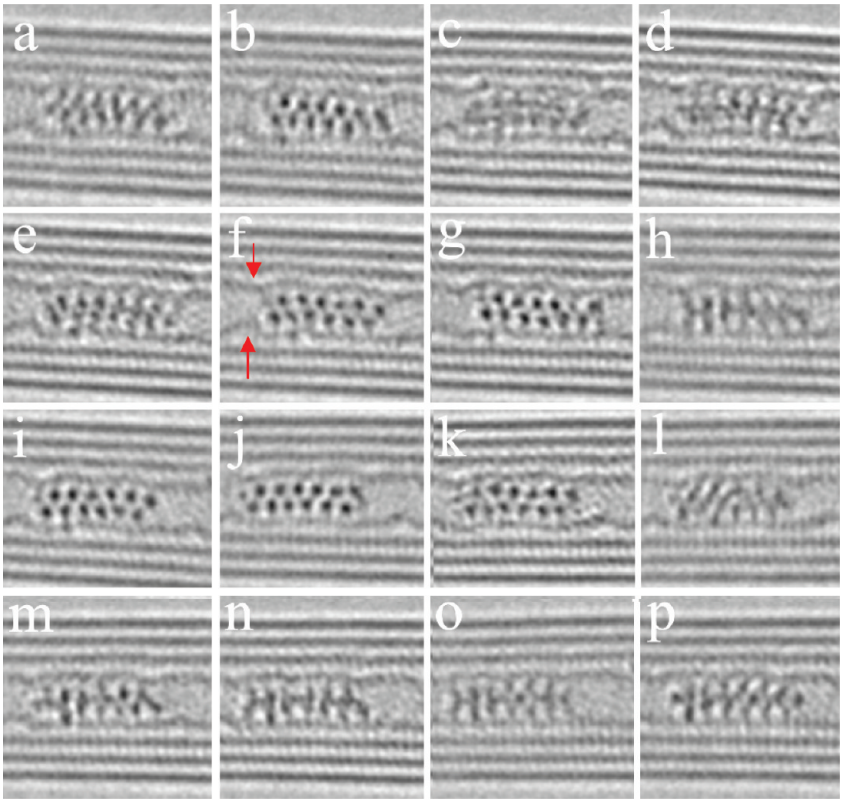

Figure 6. Time series of HRTEM images showing the atomic structural rearrangements of a Pr nanocrystal within the inner nanotube. Time between frames is 10 s. Arrows indicate narrow region of inner nanotube that restricts translational movement of the nanocrystal.

shows the end-on view of the nanocrystal in the MWNT for four different rotations. The arrow indicates a reference orientation for the nanocrystal and illustrates the rotation between each. Figure 7e−h shows the front view projection of the same structure as above, viewed in the direction of the green arrow, shown in Figure 7a. This projection was then used for the HRTEM image simulations shown in Figure 7i−l, respectively. The front half of the MWNT has been removed for clarity of presentation in Figure 7e−h but were included in the image simulations. The image simulations show the contrast from the walls of the MWNT and darker contrast from the Pr atoms. In Figure 7i, the strong contrast is due to the overlap of two Pr atoms in the projection, seen clearly in the end-on view in Figure 7a. This matches the experimental images in Figure 6b,f,g,i,j,k. As the nanocrystal is rotated about its long axis, Figure 7j−l, the contrast in the simulated images due to the Pr atoms changes. The contrast profiles in Figure 7k,l look similar to those observed experimentally in Figure 6a,d,e,h,l−p. Some slight differences are observed, which we attribute to movement of the nanocrystal during the experimental data acquisition time of 2 s and to deviation of the atoms from the perfect crystal structure. The contrast from the nanocrystal within the MWNT is also influenced by its position relative to the atomic structure of the MWNT due to the effects of overlapping carbon atoms on the contrast, and slight lateral shifts of the PrC_2 cluster within the MWNT lead to different contrast profiles in the HRTEM image simulations. Overall, however, good agreement is found between the proposed PrC_2 nanocrystal and the experimentally observed structure.

The fact that a nanocrystalline carbide phase is formed is not surprising and is most likely the reason behind the stability of the cluster as compared to the case of Dy atoms.[10] The previous report of Dy atoms showed that stable clusters are not formed, and instead, destruction of the nanotube host occurred.[10] A key component in our experiments was that we were able to observe the dynamics of nanocrystal formation due to the high concentration of metal atoms within the nanotube. The $Pr_2@C_{72}$ has two metal atoms in each cage compared to $La@C_{82}$ and $Dy@C_{82}$.[10,11] This results in a higher concentration of metal atoms being released once the coalescence begins. This significantly reduced the time required for metal atoms to pair up, form small clusters, and then coalesce to form small nanocrystals. The mobility of Pr atoms did not appear to be significantly different to La atoms during the electron beam irradiation.

From our extensive observations of metallofullerene coalescence in nanotubes under 80 kV electron beam irradiation, we have found that a crucial factor in maintaining the integrity of the nanotube host for a long duration is that it is relatively defect-free, clean from surface contamination, and isolated from other

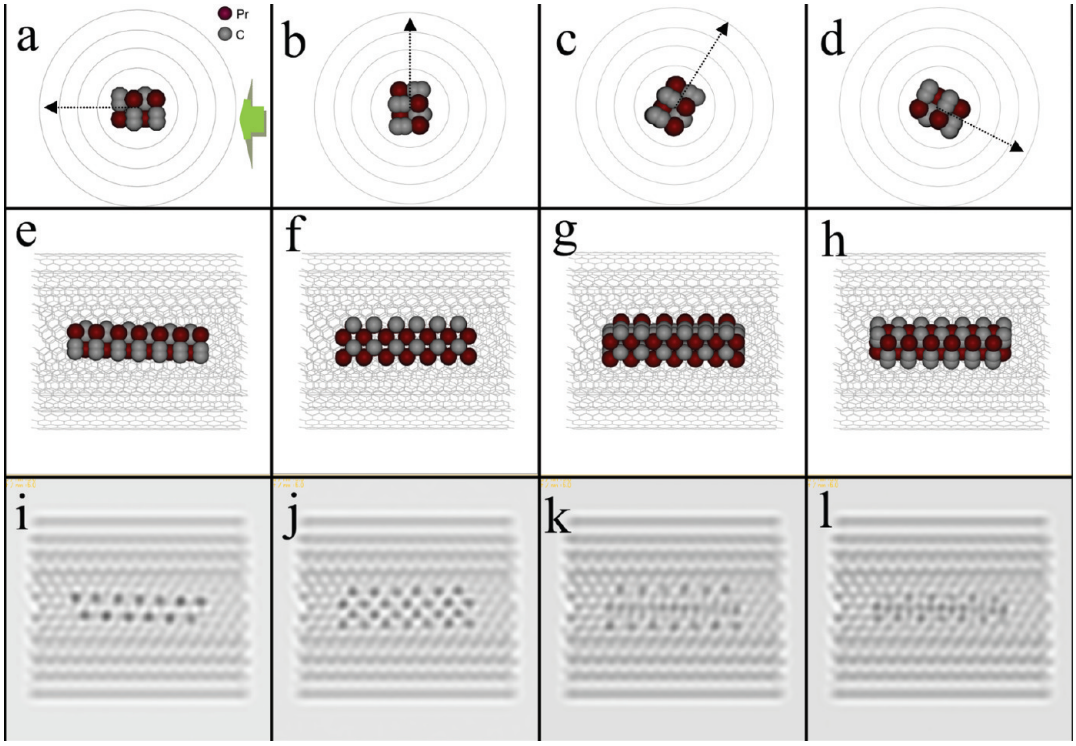

Figure 7. (a−d) End-on views of an atomic model of a PrC_2 nanocrystal inside a MWNT with different rotation. The black arrow indicates a relative orientation of the PrC_2 nanocrystal in each frame as it rotates. (e−h) Front view, shown by green arrow in (a), of the corresponding structure shown above. The front half of the MWNT has been removed for presentation purposes. (i−l) HRTEM image simulations of the atomic models presented in (e−h) for different rotation angles of the PrC_2 nanocrystal. Pr atoms red and C atoms gray.

nanotubes. We recently showed that defects and surface contamination lead to a reduction in the stability of SWNTs under 80 kV electron beam irradiation, regardless of whether they are filled with fullerenes.[34] Defects in the side wall of a peapod can provide reaction sites for the metal atoms to interact with and accelerate the destruction of the nanotube. Surface contamination on a peapod can react with the nanotube under 80 kV electron beam irradiation, leading to structural defects, which also provide sites for the metal atoms to interact with. An adjoining nanotube may also react with a peapod under 80 kV electron beam irradiation to change its structure. We used multiwalled nanotubes for peapods in our work here, and the extra walls make them more robust against destruction compared to SWNTs.

CONCLUSIONS

We have shown a preference for clustering of Pr atoms to form stable PrC_2 nanocrystals rather than remaining as single Pr atoms adhered to the side walls of carbon nanotubes. Nanocrystals formed by the coalescence of clusters and, in general, not through the atom by atom addition to a single cluster. We have also studied the dynamics of single Pr atoms *in situ* under continuous electron beam irradiation at 80 kV using atomic-resolution LV-AC-HRTEM. This demonstrates the evolution of an ordered system of fullerenes packed in a nanotube (*i.e.*, peapods), into disorder during electron beam irradiation, and then the recovery of a new ordered system through the formation of an inner nanotube and confined PrC_2 nanocrystal.

METHODS

$Pr_2@C_{72}$ metallofullerenes were prepared by the arc-discharge method with Pr-doped graphite rods and purified according to the procedures outlined in ref 28. Peapods were prepared using DWNTs and TWNTs purchased from Helix and annealed in air at 420 °C for 1 h to open the ends for filling with fullerenes. A solution containing $Pr_2@C_{72}$ in CS_2 was drop-cast onto buckypaper containing the DWNTs and TWNTs. Following CS_2 evaporation, the composite was transferred into a quartz tube, sealed under vacuum, and placed in a furnace for 4 days at 450 °C. TEM samples were prepared by dispersing the peapods in methanol using an ultrasonic bath and dipping a lacey carbon coated TEM grid into the solution. HRTEM was performed using a JEOL JEM-2200MCO field-emission gun transmission electron microscope, fitted with probe and image aberration correctors, and operated at an accelerating voltage of 80 kV. Data were recorded using a Gatan Ultrascan 4k × 4k CCD camera with 2 s acquisition times. Beam current densities of approximately 0.05 pA/nm^2 were used throughout. Electrons always irradiated the sample between frames, unless specified.

HRTEM image simulations were performed using JEMS software with supercells. The CoNTub algorithm was used to generate the nanotube structures.[35] Accelrys DS Viewer Pro was used to construct the atomic model and supercell coordinates for the $Pr_2@C_{72}$ inside the DWNT and the PrC_2 nanocrystal. Image simulation conditions for all cases used an accelerating voltage = 80 kV and Cs = −0.005 mm.

Acknowledgment. J.H.W. thanks the Violette and Samuel Glasstone Fund, Royal Society and Brasenose College for support.

REFERENCES AND NOTES

1. Britz, D. A.; Khlobystov, A. N.; Porfyrakis, K.; Ardavan, A.; Briggs, G. A. D. Chemical Reactions Inside Single-Walled Carbon Nano Test-Tubes. *Chem. Commun.* **2005,** 37–39.
2. Guan, L.; Suenaga, K.; Shi, Z.; Gu, Z.; Iijima, S. Polymorphic Structures of Iodine and Their Phase Transition in Confined Nanospace. *Nano Lett.* **2007,** *7*, 1532–1535.
3. Guan, L.; Suenaga, K.; Okubo, S.; Okazaki, T.; Iijima, S. Metallic Wires of Lanthanum Atoms Inside Carbon Nanotubes. *J. Am. Chem. Soc.* **2008,** *130*, 2162–2163.
4. Chen, S.; Kobayashi, K.; Miyata, Y.; Imazu, N.; Saito, T.; Kitaura, R.; Shinohara, H. Morphology and Melting Behavior of Ionic Liquids Inside Single-Walled Carbon Nanotubes. *J. Am. Chem. Soc.* **2009,** *131*, 14850–14856.
5. Liu, Z.; Joung, S.-K.; Okazaki, T.; Suenaga, K.; Hagiwara, Y.; Ohsuna, T.; Kuroda, K.; Iijima, S. Self-Assembled Double Ladder Structure Formed Inside Carbon Nanotubes by Encapsulation of $H_8Si_8O_{12}$. *ACS Nano* **2009,** *3*, 1160–1166.
6. Kitaura, R.; Imazu, N.; Kobayashi, K.; Shinohara, H. Fabrication of Metal Nanowires in Carbon Nanotubes *via* Versatile Nano-Template Reaction. *Nano Lett.* **2008,** *8*, 693–699.
7. Warner, J. H.; Ito, Y.; Rummeli, M. H.; Buchner, B.; Shinohara, H.; Briggs, G. A. D. Capturing the Motion of Molecular Nanomaterials Encapsulated within Carbon Nanotubes with Ultrahigh Temporal Resolution. *ACS Nano* **2009,** *3*, 3037–3044.
8. Jin, C.; Lan, H.; Suenaga, K.; Peng, L.-M.; Iijima, S. Metal Atom Catalyzed Enlargement of Fullerenes. *Phys. Rev. Lett.* **2008,** *101*, 176102.
9. Sloan, J.; Matthewman, G.; Dyer-Smith, C.; Sung, A.-Y.; Liu, Z.; Suenaga, K.; Kirkland, A. I.; Flahaut, E. Direct Imaging of the Structure, Relaxation and Sterically Constrained Motion of Encapsulated Tungsten Polyoxometalate Lindqvist Ions within Carbon Nanotubes. *ACS Nano* **2008,** *2*, 966–976.
10. Chuvilin, A.; Khlobystov, A. N.; Obergfell, D.; Haluska, M.; Yang, S.; Roth, S.; Kaiser, U. Observation of Chemical Reactions at the Atomic Scale: Dynamics of Metal-Mediated Fullerene Coalescence and Nanotube Rupture. *Angew. Chem., Int. Ed.* **2010,** *49*, 193–196.
11. Warner, J.; Ito, Y.; Rummeli, M. H.; Gemming, T.; Buchner, B.; Shinohara, H.; Briggs, G. A. D. One Dimensional Confined Motion of Single Metal Atoms Inside Double-Walled Carbon Nanotubes. *Phys. Rev. Lett.* **2009,** *102*, 195504.
12. Meyer, J. C.; Kisielowski, C.; Erni, R.; Rossell, M. D.; Crommie, M. F.; Zettl, A. Direct Imaging of Lattice Atoms and Topological Defects in Graphene Membranes. *Nano Lett.* **2008,** *8*, 3582–3586.
13. Hashimoto, A.; Suenaga, K.; Gloter, A.; Urita, K.; Iijima, S. Direct Evidence for Atomic Defects in Graphene Layers. *Nature* **2004,** *430*, 870–873.
14. Fischbein, M. D.; Drndic, M. Electron Beam Nanosculpting of Suspended Graphene Sheets. *Appl. Phys. Lett.* **2008,** *93*, 113107.
15. Girit, C. O.; Meyer, J. C.; Erni, R.; Rossell, M. D.; Kisielowski, C.; Yang, L.; Park, C.-H.; Crommie, M. F.; Cohen, M. L.; Louie, S. G.;*et al.*Graphene at the Edge: Stability and Dynamics. *Science* **2009,** *323*, 1705–1708.
16. Warner, J. H.; Rummeli, M. H.; Ge, L.; Gemming, T.; Montanari, B.; Harrison, N. M.; Buchner, B.; Briggs, G. A. D. Structural Transformations in Graphene Studied with High Spatial and Temporal Resolution. *Nat. Nanotechnol.* **2009,** *4*, 500–504.
17. Rodriguez-Manzo, J. A.; Banhart, F. Creation of Individual Vacancies in Carbon Nanotubes by Using an Electron Beam of 1A Diameter. *Nano Lett.* **2009,** *9*, 2285–2289.
18. Williams, D. B.; Carter, C. B. *Transmission Electron Microscopy. A Textbook for Materials Science*; Springer: Berlin, 2009.
19. Banhart, F. Irradiation Effects in Carbon Nanostructures. *Rep. Prog. Phys.* **1999,** *62*, 1181–1221.
20. Warner, J. H.; Ito, Y.; Zaka, M.; Ge, L.; Akachi, T.; Okimoto, H.; Porfyrakis, K.; Watt, A. A. R.; Shinohara, H.; Briggs, G. A. D. Rotating Fullerene Chains in Carbon Nanopeapods. *Nano Lett.* **2008,** *8*, 2328–2335.
21. Urita, K.; Sato, Y.; Suenaga, K.; Gloter, A.; Hasimoto, A.; Ishida, M.; Shimada, T.; Shinohara, H.; Iijima, S. Defect-Induced Atomic Migration in Carbon Nanopeapod: Tracking the Single-Atom Dynamic Behavior. *Nano Lett.* **2004,** *4*, 2452–2454.
22. Okazaki, T.; Suenaga, K.; Hirahara, K.; Bandow, S.; Iijima, S.; Shinohara, H. Real Time Reaction Dynamics in Carbon Nanotubes. *J. Am. Chem. Soc.* **2001,** *123*, 9673–9674.
23. Koshino, M.; Niimi, Y.; Nakamura, E.; Kataura, H.; Okazaki, T.; Suenaga, K.; Iijima, S. Analysis of the Reactivity and Selectivity of Fullerene Dimerization Reactions at the Atomic Level. *Nat. Chem.* **2010,** *2*, 117–124.
24. Sloan, J.; Kirkland, A. I.; Hutchinson, J. L.; Green, M. L. H. Structural Characterization of Atomically Regulated Nanocrystals Formed within Single-Walled Carbon Nanotubes Using Electron Microscopy. *Acc. Chem. Res.* **2002,** *35*, 1054–1062.
25. Kiselev, N. A.; Zakalyukin, R. M.; Zhigalina, O. M.; Grobert, N.; Kumskov, A. S.; Grigoriev, Y. V.; Chernysheva, M. V.; Eliseev, A. A.; Krestinin, A. V.; Tretyakov, Y. D.;*et al.*The Structure of 1D CuI Crystals Inside SWNTs. *J. Microsc.* **2008,** *232*, 335–342.
26. Philp, E.; Sloan, J.; Kirkland, A. I.; Meyer, R. R.; Friedrichs, S.; Hutchinson, J. L.; Green, M. L. H. An Encapsulated Helical One-Dimensional Cobalt Iodide Nanostructure. *Nat. Mater.* **2003,** *2*, 788–791.
27. Wilson, M. The Formation of Low-Dimensional Inorganic Nanotube Crystallites in Carbon Nanotubes. *J. Chem. Phys.* **2006,** *124*, 124706.
28. Plant, S. R.; Ng, T. C.; Warner, J. H.; Dantelle, G.; Ardavan, A.; Briggs, G. A. D.; Porfyrakis, K. A Bimetallic Endohedral Fullerene: $PrSc@C_{80}$. *Chem Commun.* **2009,** 4082–4084.
29. Nicholls, Sader, K.; Warner, J. H.; Plant, S. R.; Porfyrakis, K.; Nellist, P. D.; Briggs, G. A. D.; Cockayne, D. J. H. Direct Imaging and Chemical Identification of the Encapsulated Metal Atoms in Bimetallic Endofullerene Peapods. *ACS Nano* **2010,** *4*, 3943–3948.
30. Khlobystov, A. N.; Scipioni, R.; Nguyen-Manh, D.; Britz, D. A.; Pettifor, D. G.; Briggs, G. A. D.; Lyapin, S. G.; Ardavan, A.; Nicholas, R. J. Controlled Orientation of Ellipsiodal Fullerene C70 in Carbon Nanotubes. *Appl. Phys. Lett.* **2004,** *84*, 792–794.
31. Kato, H.; Taninaka, A.; Sugai, T.; Shinohara, H. Structure of a Missing-Caged Metallofullerene: $La_2@C_{72}$. *J. Am. Chem. Soc.* **2003,** *125*, 7782–7783.
32. Cowley, J. M.; Moodie, A. F. The Scattering of Electrons by Atoms and Crystals. I. A New Theoretical Approach. *Acta Crystallogr.* **1957,** *10*, 609–619.
33. Atoji, M. Magnetic and Crystal Structures of CeC_2, PrC_2, NdC_2, TbC_2, and HoC_2 at Low Temperatures. *J. Chem. Phys.* **1967,** *46*, 1891–1901.
34. Warner, J. H.; Shaffel, F.; Zhong, G.; Rummeli, M. H.; Buchner, B.; Robertson, J.; Briggs, G. A. D. Investigating the Diameter-Dependent Stability of Single-Walled Carbon Nanotubes. *ACS Nano* **2009,** *3*, 1557–1563.
35. Melchor, S.; Dobado, J. A. CoNTub: An Algorithm for Connecting Two Arbitrary Carbon Nanotubes. *J. Chem. Inf. Comput. Sci.* **2004,** *44*, 1639–1646.